

ARTICLE

Model-based evaluation of image-guided fractionated whole-brain radiation therapy in pediatric diffuse intrinsic pontine glioma xenografts

Hillary R. Husband^{1,2} | Olivia Campagne¹ | Chen He³ | Xiaoyan Zhu³ |
 Brandon M. Bianski⁴ | Suzanne J. Baker³ | Anang A. Shelat⁵ |
 Christopher L. Tinkle⁴ | Clinton F. Stewart¹

¹Department of Pharmaceutical Sciences, St. Jude Children's Research Hospital, Memphis, TN, USA

²College of Engineering and Science, Louisiana Tech University, Ruston, LA, USA

³Department of Developmental Neurobiology, St. Jude Children's Research Hospital, Memphis, TN, USA

⁴Department of Radiation Oncology, St. Jude Children's Research Hospital, Memphis, TN, USA

⁵Department of Chemical Biology and Therapeutics, St. Jude Children's Research Hospital, Memphis, TN, USA

Correspondence

Christopher L. Tinkle, Department of Radiation Oncology, St. Jude Children's Research Hospital, 262 Danny Thomas Place, MS 210, Memphis, TN 38105-3678, USA.

Email: christopher.tinkle@stjude.org

Clinton F. Stewart, Department of Pharmaceutical Sciences, St. Jude Children's Research Hospital, 262 Danny Thomas Place, Memphis, TN 38105-2794, USA.

Email: clinton.stewart@stjude.org

Funding information

This work was supported by the National Cancer Institute (CA-096832 and CA-021765), and American Lebanese Syrian Associated Charities.

Abstract

Radiation therapy (RT) is currently the standard treatment for diffuse intrinsic pontine glioma (DIPG), the most common cause of death in children with brain cancer. A pharmacodynamic model was developed to describe the radiation-induced tumor shrinkage and overall survival in mice bearing DIPG. CD1-nude mice were implanted in the brain cortex with luciferase-labeled patient-derived orthotopic xenografts of DIPG (SJDIPGx7 *H3F3A*^{WT/K27M} and SJDIPGx37 *H3F3A*^{K27M/K27M}). Mice were treated with image-guided whole-brain RT at 1 or 2 Gy/fraction 5-days-on 2-days-off for a cumulative dose of 20 or 54 Gy. Tumor progression was monitored with bioluminescent imaging (BLI). A mathematical model describing BLI and overall survival was developed with data from mice receiving 2 Gy/fraction and validated using data from mice receiving 1 Gy/fraction. BLI data were adequately fitted with a logistic tumor growth function and a signal distribution model with linear radiation-induced killing effect. A higher tumor growth rate in SJDIPGx37 versus SJDIPGx7 xenografts and a killing effect decreasing with higher tumor baseline ($p < 0.0001$) were identified. Cumulative radiation dose was suggested to inhibit the tumor growth rate according to a Hill function. Survival distribution was best described with a Weibull hazard function in which the hazard baseline was a continuous function of tumor BLI. Significant differences were further identified between DIPG cell lines and untreated versus treated mice. The model was adequately validated with mice receiving 1 Gy/fraction and will be useful in guiding future preclinical trials incorporating radiation and to support systemic combination therapies with RT.

Study Highlights

WHAT IS THE CURRENT KNOWLEDGE ON THE TOPIC?

Pharmacokinetic and pharmacodynamic models have been successfully applied to describe the effects of radiation therapy in mouse xenografts to guide the design of future preclinical studies.

This is an open access article under the terms of the Creative Commons Attribution-NonCommercial License, which permits use, distribution and reproduction in any medium, provided the original work is properly cited and is not used for commercial purposes.

© 2021 The Authors. *CPT: Pharmacometrics & Systems Pharmacology* published by Wiley Periodicals LLC on behalf of American Society for Clinical Pharmacology and Therapeutics.

WHAT QUESTION DID THIS STUDY ADDRESS?

Can we apply those models to describe the tumor progression of mice implanted with different orthotopic pediatric high-grade glioma measured with bioluminescent imaging? Can they be extended to describe the overall survival of the animals?

WHAT DOES THIS STUDY ADD TO OUR KNOWLEDGE?

The developed model adequately captured the tumor dynamics and overall survival of different gliomas xenografts and confirmed the correlation between bioluminescent imaging and survival. It allowed the quantification of the differences between the tumors in terms of tumor growth and genetic background and identified the significant impact of tumor baseline burden on the radiation killing effect.

HOW MIGHT THIS CHANGE DRUG DISCOVERY, DEVELOPMENT, AND/OR THERAPEUTICS?

The model provides useful information to guide the design of future preclinical trials incorporating radiation therapy, including dosing and tumor baseline burden selection, that will facilitate the observation of a relevant antitumor effect and the characterization of effective combination therapies.

INTRODUCTION

Pediatric high-grade gliomas (pHGGs) are highly aggressive tumors and represent about 20% of all pediatric gliomas.^{1,2} They comprise a heterogeneous group of World Health Organization grades III and IV diffuse and infiltrating tumors.^{3,4} Approximately half of pHGGs are diffuse intrinsic pontine gliomas (DIPGs), which are exclusively located in the pons, regulating many of the body's vital functions.⁵ No standard of care beyond radiation therapy (RT), traditionally delivered at 1.8 Gy/day to a cumulative dose of 54 Gy over 6 weeks, is accepted as treatment for these tumors. Despite many therapeutic attempts, pHGGs respond poorly to current treatments, with a 2-year survival outcome of less than 20%,² and DIPG remains the leading cause of brain tumor-related death in children.⁶

Although the majority of patients with DIPGs experience symptomatic improvement with RT, radiographic responses based on tumor size as assessed by magnetic resonance imaging are limited.⁷ The combination of radio-sensitizing agents with RT has the potential to significantly contribute to therapy by enhancing tumor cell kill while minimizing normal tissue toxicity. With any agent combination, the selection of the right dosing approach (e.g., relevant dosages, sequential vs. simultaneous dosing) is a significant determinant to achieve therapeutic efficacy and assess the benefit of combination versus single-agent therapy. However, identifying the best dosing approach to guide clinical investigation remains challenging as it requires multiple experiments, which is both time consuming and cost intensive. An alternative is to use mathematical modeling based on a

limited number of experiments to inform this important decision.

Pharmacokinetic and pharmacodynamic modeling has shown to be a useful tool to guide the selection of dosing regimens and support the development of novel therapeutic strategies.^{8–10} Semimechanistic models have been developed to describe tumor shrinkage induced by single-drug and combination systemic treatments^{11–14} and more recently by RT alone or combined with chemotherapy.^{15,16} Physical measurements of tumor volume/size are widely used to monitor disease progression in vivo, except for intracranial tumors for which noninvasive imaging, such as bioluminescent imaging (BLI), is a useful surrogate.^{17,18} Although BLI and tumor volume may not perfectly correlate during the time course of tumor growth, it remains the most commonly employed method for monitoring tumor dynamics and response to therapy for intracranial tumor models.¹⁸

We initially embarked on a series of clinically relevant image-guided RT dose regimens in a DIPG patient-derived orthotopic xenograft (PDOX) mouse model to determine the most appropriate RT regimen (i.e., a regimen significantly extending survival but noncurative) to optimize the evaluation of RT-drug interactions. To extend these studies across an expanding diverse set of PDOX models of DIPG and other pHGGs,^{5,19} in an efficient and practical manner, we sought to develop a pharmacodynamic model that may accurately describe the effects of RT on pHGG PDOX tumor burden and overall survival, identify treatment variables that significantly impact this effect, and ultimately be expanded to model in vivo RT-drug interactions and guide optimal preclinical RT-based combination therapies.

METHODS

Animals and tumor implantation

Preclinical studies were performed in 6 weeks or older CD1-nude mice (Charles River Laboratories) implanted with luciferase-labeled SJDIPGx7 *H3F3A*^{WT/K2M} (DIPGx7 or line 7) or SJDIPGx37 *H3F3A*^{K27M/K27M} (DIPGx37 or line 37) PDOX cells in the brain cortex originally derived from human autopsy samples as previously described.⁵ PDOXs are passaged directly into the mouse brain without *in vitro* expansion. Three studies were performed with DIPGx7 (studies L7S1, L7S2, and L7S3), and one was performed with DIPGx37 (study L37S1). Mice were maintained in a facility accredited by the Association for Assessment and Accreditation of Laboratory Animal Care. The studies were approved by the appropriate Animal Care and Use Committee and performed in accordance with the National Institutes of Health guidelines.

Whole-brain radiation and BLI

In each study, DIPG xenografts were randomized into control and treatment groups at a predefined BLI total flux threshold $>2.0 \times 10^5$ p/s after implantation. Treatment consisted in fully fractionated image-guided whole-brain radiation, performed with the Small Animal Radiation Research Platform (SARRP, Xstrahl Inc.) as described previously.²⁰ In all studies, treated mice were radiated with a dosage of 2 Gy/ay, 5 days on and 2 days off, for a total dosage of 20 Gy (10 days of treatment). In study L7S1, additional groups were radiated with 54 Gy as 2 Gy/fraction 5 days on and 2 days off (27 days), and 20 Gy as 1 Gy/fraction, 5 days on and 2 days off (20 days).

Tumor progression was measured either weekly or biweekly using BLI until moribund. Mice were anesthetized with isoflurane and injected intraperitoneally with 125 mg/kg luciferin (no. 337050500; ACROS Organics). BLI was acquired using a Xenogen IVIS System (Xenogen IVIS-200, PerkinElmer).

Pharmacodynamic modeling

Modeling strategy

Measured BLI data were divided into a model-building and validation data sets. All control animals and mice receiving RT at 2 Gy/fraction were included in the model-building data set, whereas mice treated at 1 Gy/fraction were set aside for model validation. The model included the tumor growth dynamics without treatment, the radiation-induced tumor shrinkage, and the overall survival. These three components were sequentially modeled using a population-based approach with Monolix (version 2019R2; Lixoft). Fixed-effects

and random-effects parameters were estimated with the stochastic approximation expectation maximization algorithm. Interindividual variability terms were assumed log-normally distributed and implemented using an exponential model. Proportional error models described the residual variability. Data below the limit of quantification (defined as 2.0×10^5 p/s) were censored (Beal's M3 method).²¹ Model selection and evaluation were based on statistical changes in the objective function value, precision of parameter estimates (relative standard error [RSE%]), and diagnostic plots.²² Internal validation was performed using prediction-corrected visual predictive checks (pcVPCs) based on 1000 data set replicates.²³

Tumor growth model

Different tumor growth models used to describe tumor dynamics in xenografts were tested.^{11,24} The time between tumor implantation and start of treatment differs across studies, resulting in highly variable tumor burden baselines at enrollment. Those values were used as the initial conditions of the equations describing the tumor BLI dynamics. Statistical differences between the two DIPG PDOXs were tested by including a categorical covariate on the model parameters, with criteria *p* values of 0.05.²⁵

Radiation-induced tumor shrinkage model

The parameters estimated to describe the tumor growth were fixed as Bayesian priors to model the radiation-induced killing effect. Based on the delay observed between the start of radiation and the tumor shrinkage, the following two common models were investigated: the cell distribution model¹² and the signal distribution model.¹³ The radiation input was modeled as an intravenous bolus with fast decline over time. Linear and nonlinear functions were explored to describe the radiation-killing effect. The impact of the baseline tumor BLI at enrollment was investigated as a continuous or categorical covariate on the parameters, with a criteria *p* value of 0.05.²⁵ Differences between the two DIPG PDOXs were also tested as described previously. The continuous covariate was tested as a power model scaled to the median covariate value. The categorical covariate was implemented as an exponential change. In addition, the impact of the cumulative radiation dose administered was investigated on parameters using a continuous Hill function.

Survival model

Survival was considered as a one-off event (i.e., length of time until moribund). A time-to-event model was developed

to describe the survival time distribution in all mice using parametric hazard functions.²⁴ Exponential, Weibull, log-logistic, uniform, Gompertz, and gamma hazard functions were investigated. Interindividual variability terms were tested on each parameter.

The survival model was first developed independently from the tumor dynamics. Then all the individual tumor BLI profiles, derived from the previous steps, were included to characterize the correlation between the BLI dynamics and survival. Thus, the survival baseline hazard was assumed to be a function of the tumor BLI data. Differences between DIPG cell lines, and between untreated versus treated mice, were tested as categorical covariates as previously described.

Model external validation and simulations

External model validation was performed with the cohort of mice radiated with 20 Gy at 1 Gy/fraction. Based on the RT dosing schedule and the characteristics of the validation group (e.g., cell line, median tumor burden at baseline), the fixed-effects and random-effects parameters were used to simulate the tumor BLI dynamics and the survival distribution. The model predictions of the tumor BLI dynamics (median and 90% prediction interval) were graphically compared with the observed tumor BLI data of the validation cohort. The model predictions of the overall survival for the median tumor shrinkage profile (median and 90% confidence interval) were also overlaid with the survival distribution of the validation cohort for visual assessment.

Model-based simulations were then performed for different RT dosing regimens to further evaluate the impact on the tumor dynamics and overall survival. The simulations were performed using Simulx (mlxR 4.1.4 R package).²⁶

RESULTS

Bioluminescence and survival data

Study L7S1 included a control group and three groups radiated to 20 Gy at 1 or 2 Gy/fraction or to 54 Gy at 2 Gy/fraction (six mice/group). Study L7S2 consisted of a control group and mice radiated to 20 Gy at 2 Gy/fraction (seven mice/group). Study L7S3 included a control cohort and mice radiated to 20 Gy at 2 Gy/fraction (eight mice/group). Study L37S1 comprised a control group and mice radiated to 20 Gy at 2 Gy/fraction (eight mice/group). In studies L7S1, L7S2, L7S3, and L37S1, treatment started 27, 25, 15, and 25 days after implantation, respectively, and mean tumor BLI baseline at enrollment was $3.38 \cdot 10^5$, $1.79 \cdot 10^6$, $9.26 \cdot 10^6$, and $2.18 \cdot 10^6$ p/s, respectively, 1 to 4 days before start of treatment.

The cohort treated to 20 Gy at 1 Gy/fraction in study L7S1 constituted the model validation data set (six mice). The remaining animals, that is, all control groups and mice receiving RT at 2 Gy/fraction from each study, were included in the model-building data set (64 mice), and the corresponding tumor BLI data after enrollment and survival distribution are shown in Figure 1. In the group radiated to 54 Gy, tumor BLI was measured for up to 98 days after enrollment.

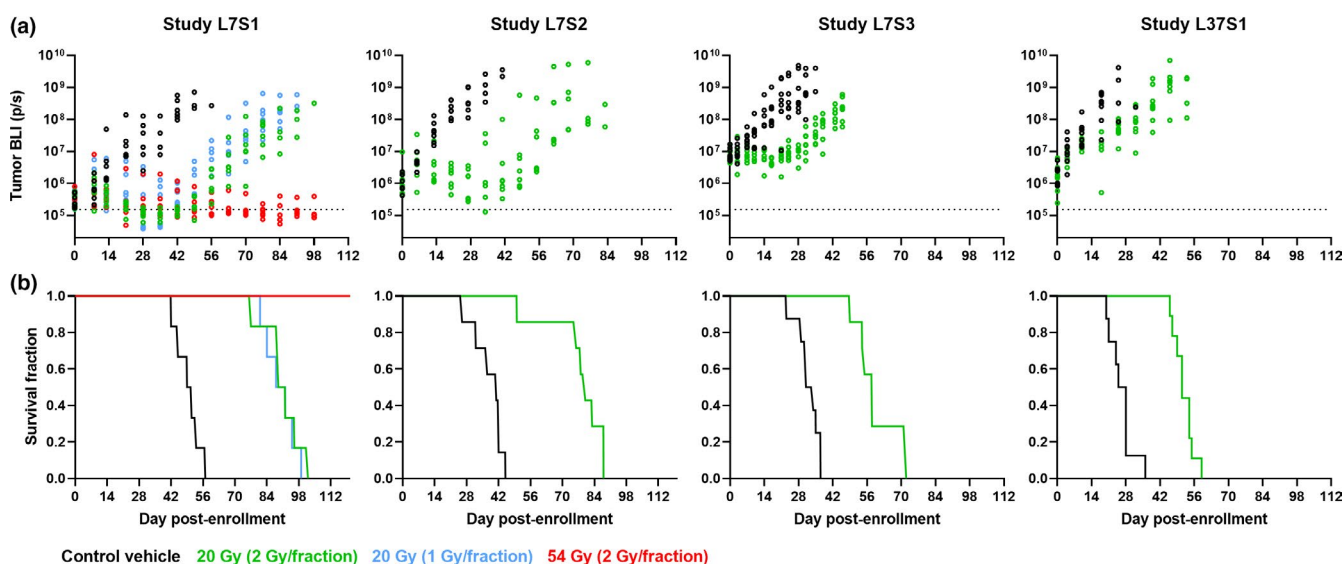


FIGURE 1 Observed bioluminescence and survival data. Observed tumor bioluminescence data versus time (a) and observed survival distribution using Kaplan-Meier plots (b) for each preclinical study. Radiation treatment was administered with a 5-days-on and 2-days-off schedule. The dotted line represents the threshold of BLI quantification used for modeling purpose ($2 \cdot 10^5$ p/s). BLI, bioluminescent imaging

Tumor growth model

The tumor BLI measurements of the untreated mice were used to develop the tumor growth model. The tumor growth dynamics were best described using a logistic growth function:

$$\frac{dTV}{dt} = k_g \cdot TV \cdot \left(1 - \frac{TV}{TV_{MAX}}\right)$$

where TV is the tumor BLI reflecting tumor volume, k_g is the tumor growth rate constant, and TV_{MAX} represents the maximum tumor volume. Interindividual variability was estimated on all parameters. A significantly faster k_g was identified in DIPGx37 xenografts (mean 0.388/day) compared with DIPGx7 animals (mean 0.205/day, Mann-Whitney $p = 0.0003$; Figure 2a). The categorical covariate (DIPGx7 vs. 37) implemented on k_g explained 25% of the variability initially observed. The parameters were well estimated with RSE% <30%. Figure 2b–d shows the model fits for representative animals in each study, diagnostic plots, and pcVPCs. The model adequately captured the data with no significant bias.

From this model, the doubling times of DIPGx7 and DIPGx37 xenografts were estimated at 3.6 ± 1 and 1.9 ± 0.62 days, respectively.

Tumor growth inhibition model

The tumor BLI measurements of the treated mice included in the model-building data set were best described using the signal distribution model with three transit compartments (Figure S1). The radiation-induced tumor killing effect was described as a linear function of the radiation dose with the rate constant k_1 . Tumor burden at baseline significantly influenced both k_1 and the transduction time τ (Figure 3a). k_1 significantly decreased with a higher tumor burden at enrollment (correlation coefficient $p = 0.0002$). Tumor baseline included as a continuous covariate on k_1 explained 39% of the variability associated with k_1 . τ was significantly lower in mice with tumor burdens at baseline greater than $4 \cdot 10^6$ p/s ($p = 0.0009$). However, in mice with lower tumor baselines, the correlation between τ and tumor BLI values was

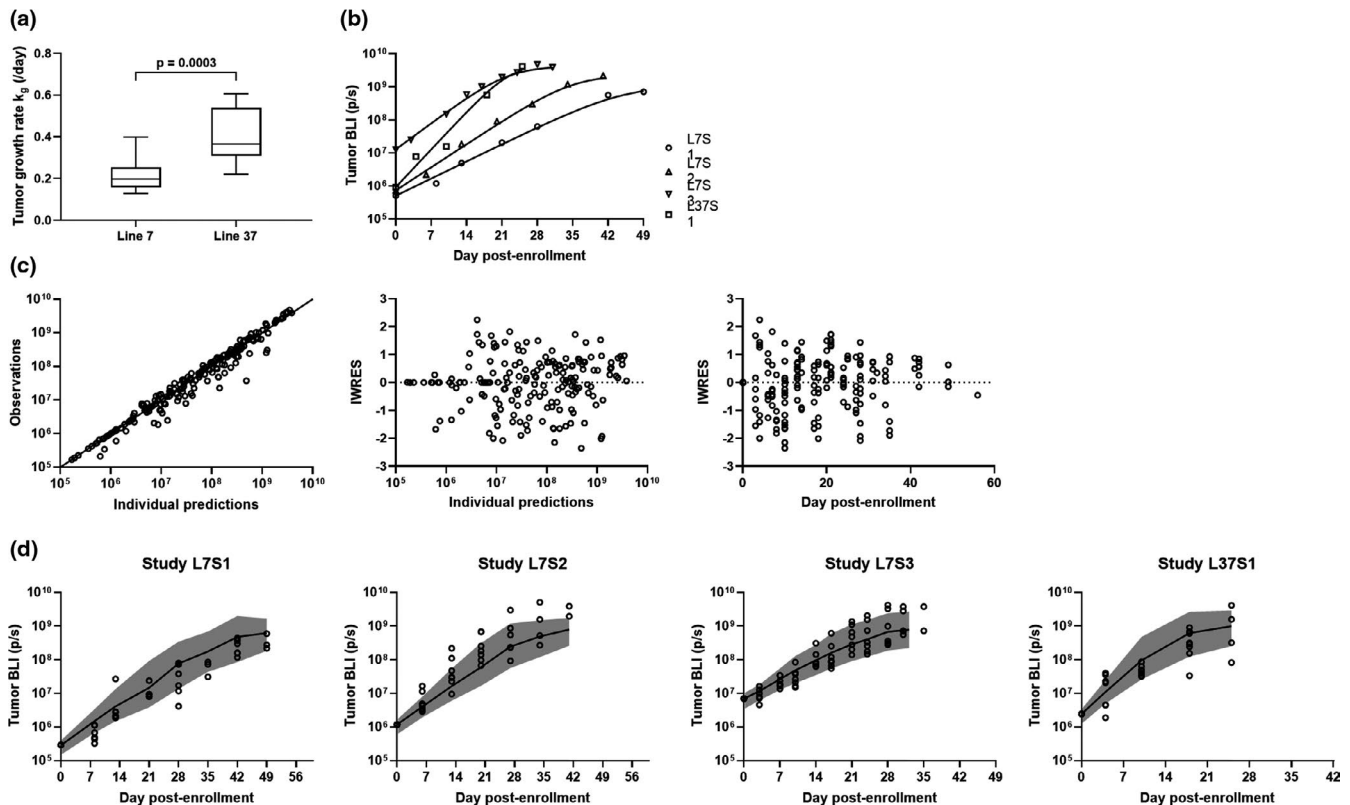


FIGURE 2 Tumor growth model fits and covariate relationships. (a) Distribution of tumor growth rates estimated in mice implanted with the diffuse intrinsic pontine glioma cell line 7 versus line 37. (b) Model predictions (solid lines) overlaid with observed data for four representative untreated mice (one selected mouse per study). (c) Goodness-of-fit plots including observed versus individual predicted values (first column), IWRES versus predictions (second column) and versus days (third column). (d) Prediction-corrected visual predictive checks stratified by preclinical study. In each graph, dots represent individual observed tumor bioluminescence data, and solid lines and shaded areas are the medians and 90th prediction intervals of the model-based simulations. BLI, bioluminescent imaging; IWRES, individual weighted residuals; k_g , tumor growth rate

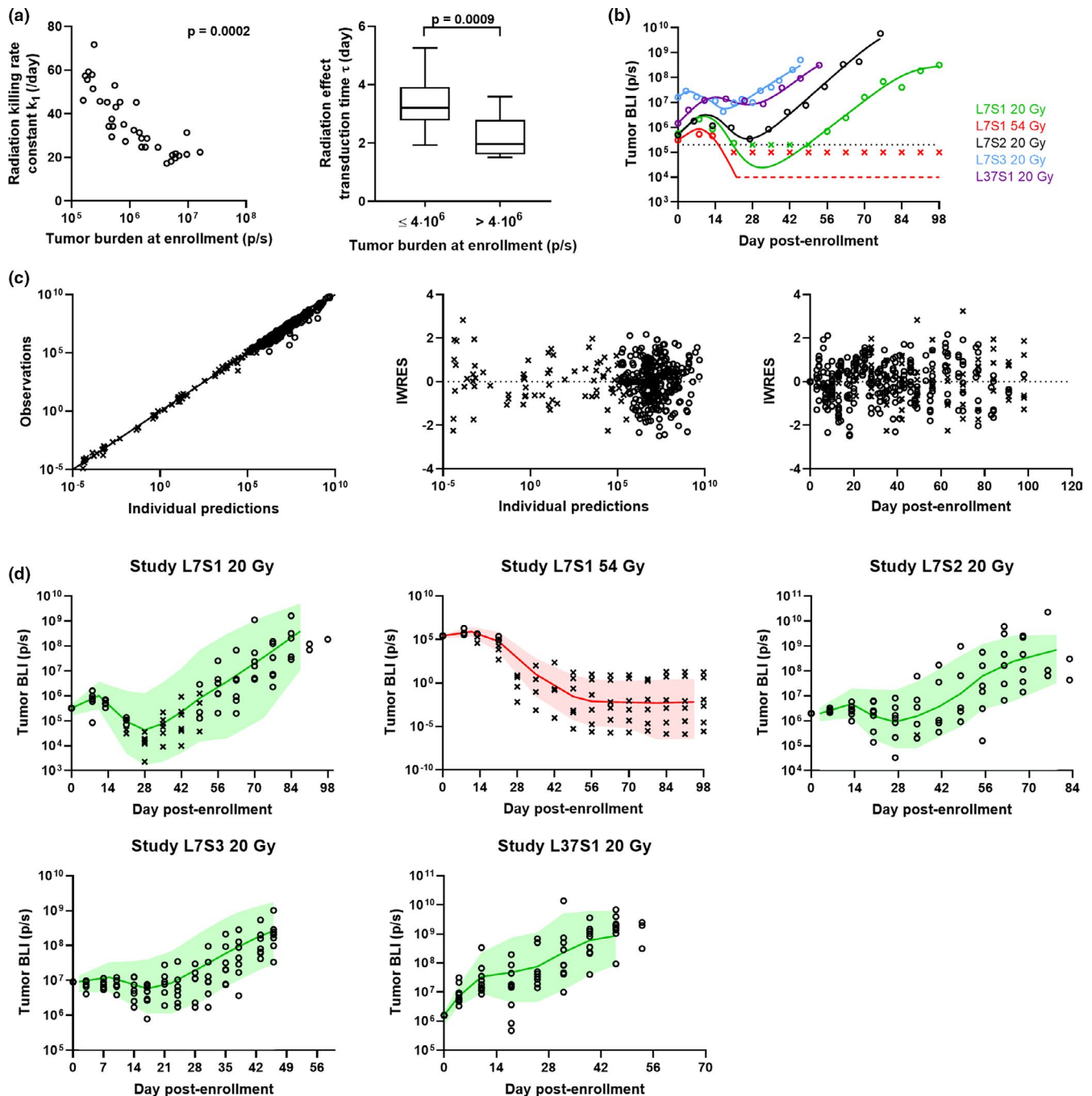


FIGURE 3 Tumor growth inhibition model fits and covariate relationships. (a) Association between the radiation-induced killing rate constant k_1 and tumor burden at baseline (first column) and distribution of radiation effect transduction time in mice with baseline tumor burden $\leq 4 \cdot 10^6$ p/s versus $> 4 \cdot 10^6$ p/s (second column). (b) Model predictions (solid lines) overlaid with observed data (circles) for representative mice treated with 20 or 54 Gy as 2 Gy per fraction. The dotted line is the threshold of quantification, crosses are data below the limit of quantification, and the dashed line reflects complete inhibition of tumor proliferation. (c) Goodness-of-fit plots including observed versus individual predicted values (first column), IWRES versus predictions (second column) and versus days (third column). (d) Prediction-corrected visual predictive checks stratified by preclinical study. Solid lines and shaded areas are the medians and 90th prediction intervals of the model-based simulations. (c,d) Crosses represent simulated observations below the limit of quantification. BLI, bioluminescent imaging; IWRES, individual weighted residuals; k_1 , radiation-induced killing rate constant

not significant. Therefore, tumor baseline was associated with τ as a categorical covariate (“high” $> 4 \cdot 10^6$ p/s vs. “low” $\leq 4 \cdot 10^6$ p/s) and explained 20% of the variability. Mice radiated to 54 Gy exhibited prolonged low BLI values,

which were considered as below the threshold of quantification. This long-term effect of RT was modeled by adding an inhibitory effect on the tumor growth rate k_g , driven by the cumulated RT dose, according to a Hill function, as follows:

$$k'_g = k_g \cdot \left(1 - \frac{\sum RT^\gamma}{IC_{50}^\gamma + \sum RT^\gamma} \right)$$

where $\sum RT$ is the cumulative RT dose, IC_{50} is the cumulative RT dose leading to a 50% inhibition of k_g estimated at 32.8 Gy, and γ is the Hill coefficient. Figure S2 depicts the shape of the inhibition curve.

No significant difference in the radiation effect parameters was identified between DIPG PDOXs. The parameters were well estimated (Table 1). Figure 3b–d shows the model fits for representative animals in each study, diagnostic plots, and pcVPCs. The model adequately characterized the central tendency and variability of the data.

Survival model

The survival distribution of all mice included in the model-building data set was first modeled independently from the tumor BLI dynamics. The survival distribution was best described with the Weibull hazard (h) function:

$$h(t) = \frac{p}{Te} \cdot \left(\frac{t}{Te} \right)^{p-1}$$

where p is the shape parameter, and Te is the median of the Weibull distribution. Interindividual variability was included on Te and was significantly influenced by two categorical covariates: treatment status (control vs. RT) and DIPG PDOX (DIPGx7 vs. 37).

TABLE 1 Final model parameter estimates

Parameter (unit)	Symbol	Estimate (RSE%)	Interindividual variability (RSE%)
Tumor growth model			
Tumor growth rate (per day)	k_g	0.388 (11.9)	0.315 (14.2)
DIPG cell line 7 effect on k_g	β_{line7}	-0.639 (21.6)	–
Maximum tumor size (p/s)	TV_{MAX}	1.44×10^9 (28)	1.06 (19.7)
Proportional residual error	ϵ_{prop}	0.39 (6.2)	–
Tumor growth inhibition model			
Radiation killing rate constant (per day)	k_1	34.9 (5.3)	0.239 (16.7)
Baseline effect coefficient on k_1	β_{base}	-0.259 (14.6)	–
Radiation effect transduction time	τ	3.29 (7.3)	0.288 (16.2)
High baseline effect coefficient on τ	$\beta_{high\ base}$	-0.46 (29)	–
Cumulative RT dose inhibiting 50% k_g (Gy)	IC_{50}	32.8 (3.5)	–
Proportional residual error	ϵ_{prop}	0.39 (5.0)	–
Survival model			
Shape parameter	p	5.3 (0.36)	–
Median Weibull distribution	Te	1320 (6.3)	0.115 (29)
DIPG cell line 7 effect on Te	β_{line7}	0.323 (19.5)	–
Treatment status effect on Te	β_{treat}	0.663 (8.3)	–

Note: Interindividual variability is reported as standard deviation.

The covariate relationships were implemented as follows: $k_{g,i} = k_g \cdot e^{\beta_{line7} \cdot LINE_i}$; $K_{1,i} = k_1 \cdot \left(\frac{Baseline_i}{843900} \right)^{\beta_{base}}$ and $\tau_i = \tau \cdot e^{\beta_{high\ base} \cdot HIGH\ BASE_i}$; $Te_i = Te \cdot e^{\beta_{treat} \cdot TREATMENT_i} \cdot e^{\beta_{line7} \cdot LINE_i}$.

where $LINE$ equals 1 for DIPGx7 and 0 otherwise, $HIGH\ BASE$ equals 1 for tumor burden baseline $>4 \cdot 10^6$ p/s and 0 otherwise, and $TREATMENT$ equals 1 for radiated mice and 0 for untreated mice. Baseline corresponds to the observed tumor baseline burden for each individual mouse.

Abbreviations: DIPG, diffuse intrinsic pontine glioma; RSE%, relative standard error.

Then the model-predicted individual tumor BLI profiles obtained previously were integrated, and the hazard baseline was modeled as a function of the BLI dynamics as follows:

$$h(t) = TV \cdot \frac{P}{Te} \cdot \left(\frac{t}{Te}\right)^{p-1}$$

After including the tumor dynamics, the model fits were improved, and the estimated interindividual variability associated with Te was decreased by 38%, confirming that tumor BLI measurements were good predictors of survival. The two previous covariates were still significant. Te estimates were lower in the control cohorts and lower in the DIPGx37 xenografts (Figure 4a). The parameters are reported in Table 1. The predictive performance of the survival model was evaluated using simulations. The observed survival distribution was reasonably predicted by the model-based simulations for each study and treatment group despite some bias for the treated mice in study L7S3 (Figure 4b).

Model external validation and simulation

Mice included in the model-validation data set received 20 Gy at 1 Gy/fraction. The model was used to simulate tumor shrinkage and survival outcomes after this radiation dosing schedule. A total of 500 simulations were performed based on the range of baseline BLI values of the validation cohort. The 50th percentile of the model tumor BLI predictions adequately matched the central tendency of the observed BLI data (Figure 5a). The observed survival distribution was well predicted by the model with an observed versus predicted median survival of 90 versus 91 days.

The validated model was used to further explore the impact of different radiation dosing schedules and tumor burden at baseline in both DIPG PDOXs. Figure 5b shows the simulated mean tumor BLI and survival profiles after a total dose of 10 Gy (2 Gy/fraction), 20 Gy (1 or 2 Gy/fraction), 39 Gy (3 Gy/fraction), and 40 Gy (5 Gy/fraction), with the same tumor burden baseline of $2.7 \cdot 10^5$ p/s. Figure 5c shows the

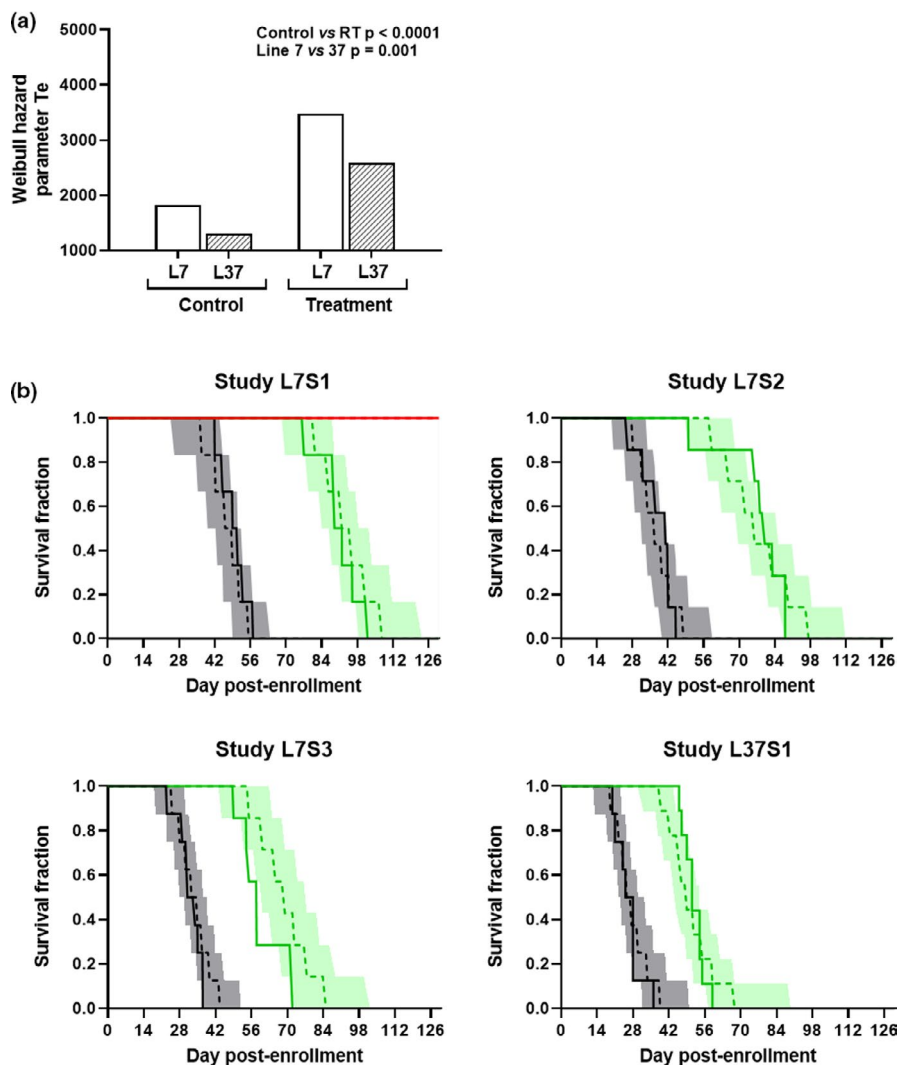
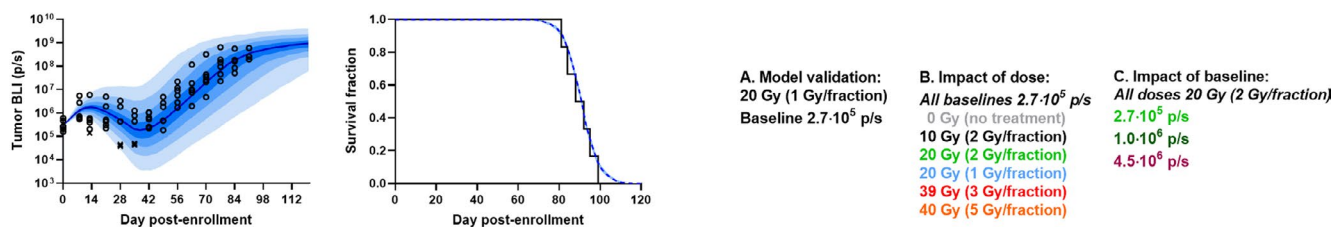
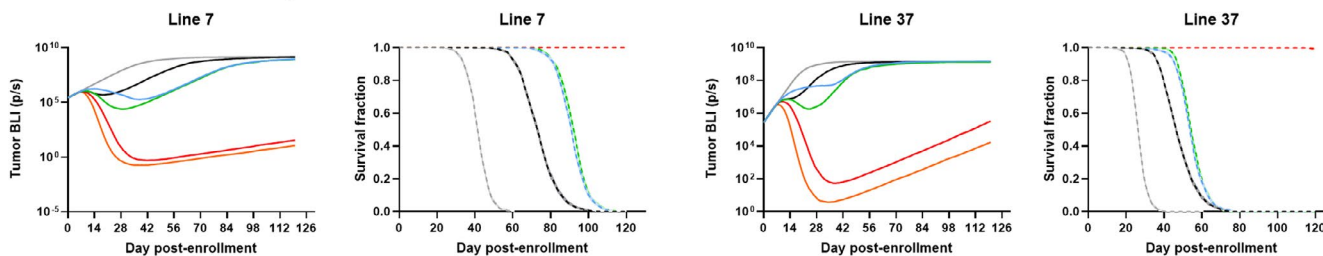


FIGURE 4 Survival model fits and covariate relationships. (a) Distribution of the Weibull hazard parameter between control and treated mice implanted with diffuse intrinsic pontine glioma lines 7 and 37. (b) Kaplan-Meier plots and visual predictive checks stratified by preclinical study. In the different panels, black, green, and red colors represent untreated mice, mice receiving 20 Gy and 54 Gy (2 Gy/fraction), respectively. Solid lines are the observed survival distribution. Dashed lines and shaded areas are the medians and 90th prediction intervals of the model-based simulations. RT, radiation therapy; Te , Weibull scale parameter

(a) External model validation



(b) Model simulations - Impact of dose



(c) Model simulations - Impact of baseline

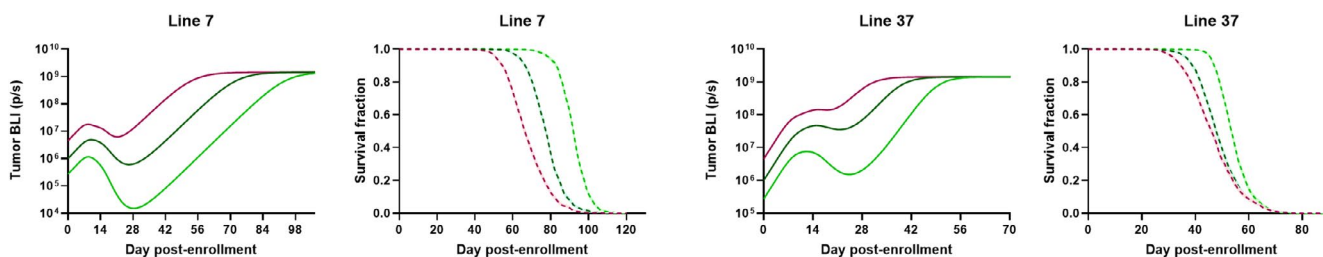


FIGURE 5 Model validation and model-based simulations. (a) Model predictions for the validation cohort receiving 20 Gy (1 Gy/fraction). Left panel: observed data (dots and crosses for data below the limit of quantification) and 90th prediction interval of model simulations (shaded area). Right panel: observed (black line) and predicted mean and 90th confidence interval of survival distribution (dashed blue line and shaded area). (b, c) Mean simulated tumor bioluminescence and survival profiles for mice implanted with DIPGx7 or DIPGx37 at different radiation dosing schedules or at different tumor burden baselines. All treatments were simulated as one fraction per day, 5 days on and 2 days off, starting on day 4. BLI, bioluminescent imaging

simulated mean tumor BLI and survival profiles after a total dose of 20 Gy (2 Gy/fraction) with different tumor burden baselines ($2.7 \cdot 10^5$ p/s, $1.0 \cdot 10^6$ p/s, or $4.5 \cdot 10^6$ p/s). All regimens were simulated as one fraction/day, 5 days on and 2 days off, starting on day 4.

DISCUSSION

The pharmacodynamic model developed in mice bearing luciferase-labeled PDOX DIPGx7 and DIPGx37 adequately described tumor progression and survival distribution after different RT regimens that resemble clinical dose fractionation schemes. A difference in the tumor growth rate was identified between the two DIPG xenografts. The radiation killing rate was not different between the two DIPG models but was significantly smaller with higher tumor burden at baseline. Tumor BLI, DIPG PDOX type, and treatment status were significant predictors of survival. This model can

now be further used to investigate different radiation dosing strategies to inform the design of future preclinical studies. It also constitutes a base framework for developing a model describing the outcomes after RT when combined with systemic therapies.

Measurable chemotherapy effects often peak days or even weeks after the first administered dose. The same delay is characteristic of tumor response to radiation as seen in the treated xenografts with a tumor shrinkage from the first radiation dose not starting until 2 weeks. The signal distribution model selected to describe the radiation-induced effect has been commonly used to capture long delayed chemotherapy-induced tumor shrinkage.^{11,13,27} More complex models have been developed to describe radiation effects, including a model by Cardilin and colleagues.^{15,28} A noteworthy component of their model is the linear-quadratic equation to quantify the radiation-induced damages. The Cardilin model was explored using our data, although we failed to obtain model fits as good as with our own model structure, which

is less mechanistic but much less complex and thus may be more suitable for highly variable data such as our BLI measurements.

A common feature between our model and the Cardilin model is the inclusion of a long-term radiation-induced effect on the tumor growth rate along with the cell-killing effect.²⁸ In our studies, mice receiving 54 Gy exhibited low BLI measurements until 98 days after enrollment and were still alive after 130 days (Figure 1). This prolonged tumor suppression suggested that 54 Gy was curative for these mice. To model this effect, we assumed that cumulative radiation leading to extensive tumor shrinkage progressively inhibited the capacity for tumor repopulation using a typical Hill function. One potential explanation supporting an altered tumor growth rate is the change in tumor vascularization and microenvironment caused by radiation.^{29,30} After a cumulative dose of 54 Gy, a close to complete inhibition of the tumor growth rate was achieved, resulting in prolonged low BLI predictions (Figure S2). We had BLI data after 54 Gy dosing for the DIPGx7 but not for the DIPGx37 xenografts. Thus, our estimated IC_{50} of the cumulative radiation dose inhibition effect may not represent the “true” IC_{50} value for DIPGx37 xenografts.

The impact of the tumor burden at baseline on the extent of radiation-induced killing effect was an important finding. A larger tumor burden at baseline significantly decreased the radiation killing rate for the same total dose and fractionation. In addition, a tumor burden $>4 \cdot 10^6$ p/s before treatment started decreased the transduction time, that is, the length of the radiation effect. As shown by our simulations (Figure 5c), radiating mice that have large differences in tumor burden baseline with the same dose and fractionation can result in significant differences in tumor shrinkage and survival. This is critical to consider when comparing different dosing regimens and therapeutic agents to properly assess the advantage of RT. The high $4 \cdot 10^6$ p/s value was empirically selected based on the observed data. Although it should not be considered as a strict threshold, it can still guide the course of future studies. Generally, our model could now be used to further inform the design of studies in DIPG xenografts by determining a desired range of BLI values before beginning RT and by predicting the time to reach these values. The impact of tumor size on RT effect has been previously observed in clinic for other tumors.^{31,32} Larger tumors containing larger amounts of hypoxic cells more resistant to irradiation could possibly explain this phenomenon. It was suggested that chemotherapy or other interventions be applied before radiotherapy to decrease tumor size and enhance radiation effect. Although resection is generally not feasible for patients with DIPGs and currently effective systemic therapy remains elusive, the observation of this relationship may be informative for guiding future preclinical drug-radiation studies if more efficacious agents are identified.⁴

Another interesting result is the significant difference in tumor growth rate between the two DIPG cell lines without a difference in the radiation killing rate parameter. The two DIPG cell lines used in this study differ, at least in part, by their TP53 status: DIPGx7 harbors a pathogenic *TP53* mutation and DIPGx37 is wild type for *TP53*. Recently, *TP53* mutations were shown to drive DIPG resistance to RT in vitro and in patients.³³ In contrast, in our study, by only observing the BLI measurements collected in mice receiving 20 Gy (Figure 1), one could see the smaller impact of RT on the BLI profiles and the inferior survival in the study using DIPGx37 compared with those using DIPGx7. Our modeling analysis first showed in the control groups that the tumors of *TP53* wild-type DIPGx37 xenografts grew faster than that of mutant DIPGx7 xenografts. This was still observed in the radiated animals. The lack of difference between the DIPG lines regarding the radiation killing rate suggests that the smaller effect of radiation on DIPGx37 xenografts may be more driven by proliferative differences than an acquired resistance to RT. This is currently being further investigated with in vitro studies evaluating the effect of RT on the cell cycle of pediatric glioma cells.

BLI is widely performed to monitor tumor progression in vivo when the localization of the tumor does not allow the use of conventional nonimaging methods such as direct caliper measurements. BLI signals have shown a good correlation with actual tumor sizes, although some discrepancies may occur with very large tumor volumes.¹⁸ Our model was extended to include the prediction of survival distributions, a clinically relevant outcome. Our analysis showed that the BLI data and survival end points were significantly associated. This confirmed that BLI was a good predictor survival in our DIPG xenograft models.

Our model was validated for both the tumor dynamics and overall survival of DIPGx7 xenografts receiving a different RT fractionation and can now be used to further investigate other radiation dosing strategies. In particular, the model can inform optimal radiation dosing strategies to use in the context of combination therapies. In terms of extrapolation to humans, it is known that radiation alone has rarely achieved lasting remission or long-term survival in pediatric patients with DIPGs. Thus, a commonly explored clinical therapeutic strategy has been to explore drug-radiation combinations to identify synergistic relationships.¹⁵ To model this strategy preclinically, it is critical to identify an RT dosing schedule that allows the researcher to observe drug-radiation synergy, additivity, or antagonism. The selected RT dosing schedule needs to be sufficiently effective alone, but not curative, as 54 Gy was in our L7S1 study. Selecting a radiation dosing regimen (i.e., total dose and fractionation) that is clinically relevant in terms of current standard of care still remains challenging, and we believe that the model developed here can guide this decision to

optimize the future preclinical studies evaluating combination therapies. This was the primary purpose of our analysis: providing a framework to determine optimal conditions (e.g., radiation dosing, initial tumor burden to reach) across various DIPG xenograft models to use in conjunction with systemic therapy to enhance the evaluation of new treatments for pediatric brain tumors rather than providing direct clinical predictions.

The analysis has several limitations. Most of the studies were performed in DIPGx7 xenografts. Additional data using DIPGx37 xenografts would allow for confirmation of the observed differences observed in the tumor growth rates between DIPGx7 and DIPGx37 xenografts. The long-term effect of RT on the tumor growth rate was not observed in DIPGx37 xenografts, and thus the estimated IC_{50} should be interpreted carefully for those mice. Additional data from DIPGx7 xenografts with intermediate cumulative RT doses between 20 Gy and 54 Gy might also improve the characterization of the IC_{50} . Toxicity was not investigated here; however, the motivation of the study was to characterize tumor shrinkage with various radiation regimens, and the determination of a maximum tolerated dose schedule was not considered. Finally, the current model was not designed here to provide direct clinical predictions. Our immediate goal was to inform and optimize the preclinical evaluation of new therapeutic strategies including RT. The inclusion of more mechanistic processes, such as cell cycle and DNA repair capacity, is currently under investigation. By integrating these cellular end points observed across a broad selection of pHGG PDOXs and derived cell line models in to our model, the influence of driver mutations (i.e., histone H3, *TP53*, *PDGFRA*) can be evaluated and potentially used to predict mutation-specific drug class dependencies when combined with concurrent RT. Although the evaluation of similar clinical data may also be useful to develop this objective, unfortunately to date no systemic agent has been identified that consistently improves outcomes. Despite numerous attempts at varying RT regimens and/or techniques, outcomes have remained stagnant, highlighting the need to better understand the cellular effects of RT and to identify genetic liabilities and systemic agents that may exploit these effects.

This is the first time that radiation-killing effect has been explicitly modeled in pediatric DIPG xenografts and can provide useful information to guide the design of future preclinical trials incorporating RT. Given radiation remains the only therapy that consistently provides clinical responses in DIPGs, albeit in a temporary and ultimately unsatisfactory fashion, future studies including more mechanistic models of the in vivo effects of fractionated RT and drug-radiation combination therapy are desperately needed to define promising strategies that may increase the therapeutic ratio of this treatment modality.

CONFLICT OF INTEREST

The authors declared no competing interest for this work.

AUTHOR CONTRIBUTIONS

H.H., O.C., and C.L.T. wrote the manuscript. C.L.T., C.F.S., S.J.B., and A.A.S. designed the research. C.H., X.Z., and B.M.B. performed the research. H.H. and O.C. analyzed the data.

REFERENCES

1. Jones C, Karajannis MA, Jones DTW, et al. Pediatric high-grade glioma: biologically and clinically in need of new thinking. *Neuro Oncol.* 2017;19:153-161.
2. Sarkar C, Purkait S, Pathak P, Jha P. Pediatric high grade glioma. In: Somasundaram K, ed. *Advances in Biology and Treatment of Glioblastoma*. Cham: Springer International Publishing; 2017:241-266.
3. Sturm D, Pfister SM, Jones DTW. Pediatric Gliomas: Current Concepts on Diagnosis, Biology, and Clinical Management. *J Clin Oncol.* 2017;35:2370-2377.
4. Fangusaro J. Pediatric high grade glioma: a review and update on tumor clinical characteristics and biology. *Front Oncol.* 2012;2:105.
5. Silveira AB, Kasper LH, Fan Y, et al. H3.3 K27M depletion increases differentiation and extends latency of diffuse intrinsic pontine glioma growth in vivo. *Acta Neuropathol.* 2019;137:637-655.
6. Vanan MI, Eisenstat DD. DIPG in children - What can we learn from the past? *Front Oncol.* 2015;5:237.
7. Vanan MI, Eisenstat DD. Management of high-grade gliomas in the pediatric patient: Past, present, and future. *Neurooncol Pract.* 2014;1:145-157.
8. Danhof M, de Lange EC, Della Pasqua OE, Ploeger BA, Voskuyl RA. Mechanism-based pharmacokinetic-pharmacodynamic (PK-PD) modeling in translational drug research. *Trends Pharmacol Sci.* 2008;29:186-191.
9. Rajman I. PK/PD modelling and simulations: utility in drug development. *Drug Discovery Today.* 2008;13:341-346.
10. Miller R, Ewy W, Corrigan BW, et al. How modeling and simulation have enhanced decision making in new drug development. *J Pharmacokinet Pharmacodyn.* 2005;32:185-197.
11. Ribba B, Holford NH, Magni P, et al. A review of mixed-effects models of tumor growth and effects of anticancer drug treatment used in population analysis. *CPT Pharm Sys Pharmacol.* 2014;3(5):113.
12. Simeoni M, Magni P, Cammia C, et al. Predictive pharmacokinetic-pharmacodynamic modeling of tumor growth kinetics in xenograft models after administration of anticancer agents. *Cancer Res.* 2004;64:1094-1101.
13. Lobo ED, Balthasar JP. Pharmacodynamic modeling of chemotherapeutic effects: application of a transit compartment model to characterize methotrexate effects in vitro. *AAPS PharmSci.* 2002;4:E42.
14. Koch G, Walz A, Lahu G, Schropp J. Modeling of tumor growth and anticancer effects of combination therapy. *J Pharmacokinet Pharmacodyn.* 2009;36:179-197.
15. Cardilin T, Almquist J, Jirstrand M, et al. Model-based evaluation of radiation and radiosensitizing agents in oncology. *CPT Pharm Sys Pharmacol.* 2018;7:51-58.

16. Ribba B, Kaloshi G, Peyre M, et al. A tumor growth inhibition model for low-grade glioma treated with chemotherapy or radiotherapy. *Clin Cancer Res.* 2012;18:5071-5080.
17. Tuli R, Surmak A, Reyes J, et al. Development of a novel pre-clinical pancreatic cancer research model: bioluminescence image-guided focal irradiation and tumor monitoring of orthotopic xenografts. *Translational oncology.* 2012;5:77-84.
18. Jost SC, Collins L, Travers S, Piwnica-Worms D, Garbow JR. Measuring brain tumor growth: combined bioluminescence imaging-magnetic resonance imaging strategy. *Mol Imaging.* 2009;8:245-253.
19. Dunphy PS, Xu K, Gentry DT, et al. Abstract 6144: St. Jude pediatric brain tumor portal: Cloud-based resource for patient-derived orthotopic xenograft (PDOX) models of pediatric high-grade glioma, ependymoma, and CNS embryonal tumors. *Can Res.* 2020;80:6144.
20. Nimmervoll BV, Boulos N, Bianski B, et al. Establishing a pre-clinical multidisciplinary board for brain tumors. *Clin Cancer Res.* 2018;24:1654-1666.
21. Beal SL. Ways to fit a PK model with some data below the quantification limit. *J Pharmacokinet Pharmacodyn.* 2001;28:481-504.
22. Nguyen TH, Mouksassi MS, Holford N, et al. Model evaluation of continuous data pharmacometric models: Metrics and graphics. *CPT Pharm Sys Pharmacol.* 2017;6:87-109.
23. Bergstrand M, Hooker AC, Wallin JE, Karlsson MO. Prediction-corrected visual predictive checks for diagnosing nonlinear mixed-effects models. *The AAPS J.* 2011;13:143-151.
24. Mould DR, Walz AC, Lave T, Gibbs JP, Frame B. Developing exposure/Response models for anticancer drug treatment: Special considerations. *CPT Pharm Sys Pharmacol.* 2015;4(1):12-27.
25. Joerger M. Covariate pharmacokinetic model building in oncology and its potential clinical relevance. *The AAPS Journal.* 2012;14:119-132.
26. Lavielle M. mlxR: simulation of longitudinal data. R package version 4.1.4. 2020. <http://simulx.webpopix.org>. Accessed October 19 2020.
27. Yang J, Mager DE, Straubinger RM. Comparison of two pharmacodynamic transduction models for the analysis of tumor therapeutic responses in model systems. *The AAPS Journal.* 2010;12:1-10.
28. Cardilin T, Almquist J, Jirstrand M, et al. Modeling long-term tumor growth and kill after combinations of radiation and radiosensitizing agents. *Cancer Chemother Pharmacol.* 2019;83:1159-1173.
29. Barker HE, Paget JT, Khan AA, Harrington KJ. The tumour microenvironment after radiotherapy: mechanisms of resistance and recurrence. *Nat Rev Cancer.* 2015;15:409-425.
30. Tsai JH, Makonnen S, Feldman M, et al. Ionizing radiation inhibits tumor neovascularization by inducing ineffective angiogenesis. *Cancer Biol Ther.* 2005;4:1395-1400.
31. Nervi C, Arcangeli G, Badaracco G, et al. The relevance of tumor size and cell kinetics as predictors of radiation response in head and neck cancer. A randomized study on the effect of intraarterial chemotherapy followed by radiotherapy. *Cancer.* 1978;41:900-906.
32. O'Donoghue JA, Bardies M, Wheldon TE. Relationships between tumor size and curability for uniformly targeted therapy with beta-emitting radionuclides. *J Nucl Med.* 1995;36:1902-1909.
33. Werbrouck C, Evangelista CCS, Lobon-Iglesias MJ, et al. TP53 pathway alterations drive radioresistance in diffuse intrinsic pontine gliomas (DIPG). *Clin Cancer Res.* 2019;25:6788-6800.

SUPPORTING INFORMATION

Additional supporting information may be found online in the Supporting Information section.

How to cite this article: Husband HR, Campagne O, He C, et al. Model-based evaluation of image-guided fractionated whole-brain radiation therapy in pediatric diffuse intrinsic pontine glioma xenografts. *CPT Pharmacometrics Syst. Pharmacol.* 2021;10:599–610. <https://doi.org/10.1002/psp4.12627>